Using Point-Spread Functions to Identify and Characterize Unresolved Binary Brown Dwarfs

Elora N. Salway

A senior thesis submitted to the faculty of
Brigham Young University
in partial fulfillment of the requirements for the degree of

Bachelor of Science

Dr. Denise C. Stephens, Advisor

Department of Physics and Astronomy

Brigham Young University

April 2015

ABSTRACT

Using Point-Spread Functions to Identify and
Characterize Unresolved Binary Brown Dwarfs

Elora N. Salway
Department of Physics and Astronomy, BYU
Bachelor of Science

The Hubble Space Telescope (HST) has observed a fair number of brown dwarfs which, in ground based images, appear to be single objects. Frequently, however, the higher angular resolution of HST reveals that some of these objects are binary systems. The small angular separation of these binaries hints that there may be many more unresolved binary brown dwarfs observed with HST. With Point-Spread Function (PSF) fitting, it is possible to identify binary brown dwarf candidates in the HST archives which are not visually resolved according to the Rayleigh criterion. By fitting a double PSF to each brown dwarf image in each filter and camera for which data exists, we can determine a range of fluxes for both components of the binary system. These fluxes will be used to constrain theoretical spectrum of brown dwarfs to the original data to find a range of temperature and gravity for both objects. This thesis presents the results of PSF fitting for the brown dwarf 2M 0559, which reveals the object to be a strong binary candidate.

Keywords: brown dwarf, low-mass, binary, infrared, Hubble Space Telescope, point-spread function, 2MASS J05591914-1404488

ACKNOWLEDGMENTS

I acknowledge and thank the Brigham Young University Physics Department for providing funding and support for this research. In addition, I would like to acknowledge two HST Grants, GO9386 and AR11238, which funded research and preliminary work which lead to this project.

I would also like to thank prior research advisors who helped me develop the skills I needed to complete this project. Dr. Eric Hintz took a risk by giving a research opportunity to a sophomore soon leaving on a mission. Early exposure to research and data analysis helped me to develop a deep love for astronomy and what can be done with simple images of stars. J. Lewis Fox, my REU advisor at the National Solar Observatory, has been both a mentor and a friend. I will always remember the cloudy day that was dedicated to studying the chronograph which was used to complete the research.

In addition, much gratitude is extended to Dr. Denise C. Stephens for giving me the opportunity to participate in this project. She guided like a coach, helping me to recognize what I already knew. I am also grateful to Doug Gardner, who developed the Monte-Carlo testing program to demonstrate that the results of this project were viable.

Finally, I cannot overestimate the influence of my parents. When I chose to study astronomy, they supported me completely. I know they are always willing to offer guidance and assistance; but more importantly, they have taught me all I need to know to guide myself.

Contents

Table of Contents iv

List of Figures vi

1 Introduction 1
- 1.1 Intro . . . 1
- 1.2 Brown Dwarfs . . . 2
  - 1.2.1 Description . . . 2
  - 1.2.2 Prediction and Discovery . . . 3
  - 1.2.3 Classifications . . . 3
- 1.3 The Cooling Model . . . 5
  - 1.3.1 Current Theory of Cooling . . . 5
  - 1.3.2 Mass and Binary Systems . . . 7
  - 1.3.3 Point-Spread Functions . . . 7
- 1.4 Brown Dwarf 2M 0559 . . . 8
- 1.5 Previous Work at Brigham Young University . . . 9
- 1.6 Overview . . . 10
  - 1.6.1 Procedures . . . 10
  - 1.6.2 Results and Conclusions . . . 10

2 Procedures 11
- 2.1 Preparing Data for Analysis . . . 11
  - 2.1.1 Data Collection . . . 11
  - 2.1.2 Preparation . . . 13
- 2.2 Procedure for a Binary PSF Fit . . . 14
  - 2.2.1 Weighting . . . 14
  - 2.2.2 Positioning the Binary Fit . . . 15
- 2.3 Procedure for a Singular PSF Fit . . . 15
- 2.4 Use of Data from Both Procedures . . . 16
  - 2.4.1 Comparison . . . 16
  - 2.4.2 Preliminary Analysis . . . 16
- 2.5 Reliability of the Procedures . . . 16

3 Results and Conclusions **18**
3.1 2M 0559 is a Strong Binary Candidate 18
3.2 Magnitude and Spectra of 2M 0559 22
3.3 Conclusions 24
3.4 Direction for Further Work 24

Bibliography **26**

Index **28**

List of Figures

1.1 Spectra from M dwarf star, L dwarfs, T dwarfs, and Jupiter 4

1.2 Changes in luminosity over time for stars, brown dwarfs, and planets 6

2.1 Region of interest 13

3.1 Original image of 2M 0559 from NICMOS1 and residuals after analysis 20

3.2 Original image of 2M 0559 from NICMOS2 and residuals after analysis 20

3.3 An image set of 2M 0559 with logarithmic scaling 21

3.4 An image set of 2M 0337 for comparison with the 2M 0559 21

3.5 Magnitudes of binary system 22

3.6 Spectrum of 2M 0559 compared to spectra of other dwarfs 23

List of Tables

2.1 Available data sets for 2M 0559 12

3.1 χ^2 Value Comparisons 19

Chapter 1

Introduction

1.1 Intro

When you look into the night, you have the opportunity to see two familiar groups of objects, stars and planets. Yet there is another, almost invisible group of objects which creates a bridge between the smallest of stars and the largest of planets. These are the brown dwarfs. Discovered only 20 years ago, astronomers are still seeking to characterize and create models for brown dwarfs.

My research has focused on determining if one particular object, Brown Dwarf 2MASS J05591914-1404488 (2M 0559), is actually a binary system. If 2M 0559 actually consists of two brown dwarfs which orbit each other, we can characterize both objects and create more data to eventually develop an accurate evolutionary model for brown dwarfs. The remainder of Chapter 1 describes brown dwarfs, presents problems with current models of these objects, and outlines the remainder of this thesis.

1.2 Brown Dwarfs

1.2.1 Description

Brown dwarfs hold a unique position between stars and planets.

Stars vary widely in size, temperature, luminosity, and even color. Despite all these differences, each star represents a balancing point between gravity and pressure. A star begins life as a large cloud of gas collapsing upon itself. As gravity pulls the gas inward, energy builds, creating heat in the very center of the cloud. Eventually, the growing energy and density provide the perfect condition to ignite nuclear fusion in the core of the star, referred to as core-fusion. The star fuses hydrogen into helium, creating light, energy, and pressure which radiate outward. The pressure and gravity balance out, preventing the gas from collapsing anymore and creating a star. The core-fusion continues through the majority of the life of the star, allowing the temperature and luminosity to remain fairly constant.

Planets form around stars. In the later stages of the formation of the star, a disk of dust and gas surrounds the star. As the dust swirls around the star, it begins to clump together, slowly growing into pebbles and rocks. Eventually, some rocks have enough mass to develop atmospheres, the gases being held by the gravity of the newly formed planets.

Brown dwarfs develop similarly to stars, but the clouds of gas from which they form are less massive. With less mass, the energy in the center of brown dwarfs never reaches the conditions necessary to allow nuclear fusion of hydrogen to begin in the core. The lower limit of mass which can provide the necessary conditions for a star to have core-fusion range between 0.07 Solar Masses($M_\odot$) and 0.09 $M_\odot$, or approximately eighty times the mass of Jupiter (Kumar 1963). Ranging between ten and eighty times the mass of Jupiter, brown dwarfs are unable to fuse hydrogen and maintain their own source of light and energy. Many brown dwarfs have a great deal of residual heat from formation, so they still emit light, much of which is only visible in infrared

wavelengths. Since there is no core-fusion, brown dwarfs will cool and dim over time, much as an ember pulled from a fire would.

1.2.2 Prediction and Discovery

Shiv S. Kumar first presented the theory of brown dwarfs in his 1963 paper, where he gave them the name "degenerate stars." He determined that, for masses less than approximately 0.09 $M_{\odot}$, the stars no longer heat up as they contract because their interiors become degenerate (Kumar 1963). For a gas to become degenerate, the atoms need to be so close together that the Pauli Exclusion principle begins to contribute substantially to the pressure. Pressure is no longer dependent on just volume and temperature, as it would be for an ideal gas. The electron repulsion stops the collapse before the temperature rises enough to allow for core-fusion. For larger stars, as the star compresses, the temperature and pressure in the core of the star also increase, eventually providing the right environment to begin fusing hydrogen before the core of the star can reach degenerate pressures.

The first confirmed observations of brown dwarfs occurred in the late 1990s. In 1999, using data from the 2-Micron All-Sky Survey (2MASS) Kirkpatrick *et al.* located 60 potential brown dwarf candidates. They then used the Low Resolution Imaging Spectrograph (LRIS) to gather spectra of these 60 objects, as well as the spectra of an additional 6 brown dwarf candidates which were known at the time. Kirkpatrick *et al.* located features in the spectra of 26 of the objects which were absent from spectra of M type stars, which are the smallest and coolest stars. Using these spectra, Kirkpatrick *et al.* defined the L spectral class for brown dwarfs (Kirkpatrick et al. 1999).

1.2.3 Classifications

There are three classes of brown dwarfs, labeled L, T, and Y. These labels are known as the spectral classification of an object. This classification is based on the appearance of a star's spectral en-

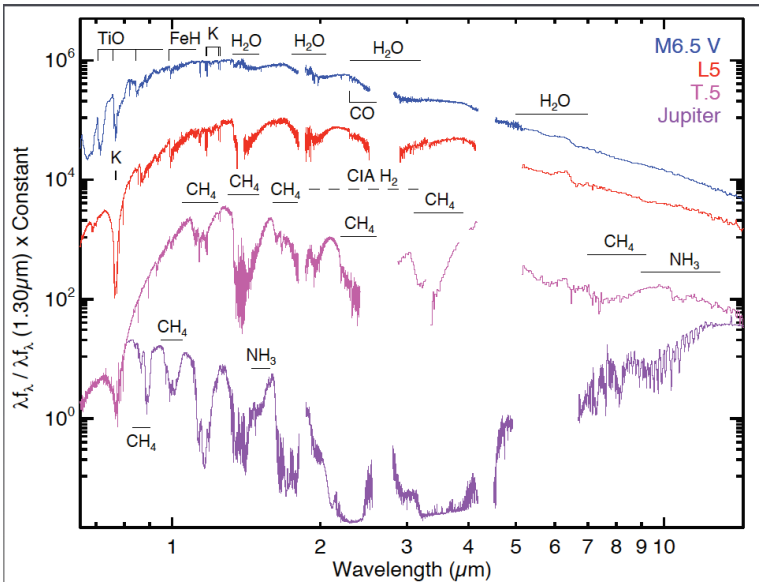

Figure 1.1 A comparison of the spectra from various objects. The uppermost spectrum is an M star, the smallest of the stars. Below that is an L dwarf, then a T dwarf. The lowest spectrum is from the planet Jupiter. Gaps in the spectra are a result of the atmosphere of the Earth blocking particular wavelengths of light. Figure has been modified from (Marley & Leggett 2009)

ergy distribution, called a spectrum. Features within a spectrum depend primarily on temperature. Unlike main sequence stars, which maintain a relatively constant spectral classification as long as they are fusing hydrogen in their core, the spectral type of a brown dwarf will change over time. As the brown dwarf cools, it moves from earlier to later spectral types, in other words, the dwarf's spectral type will change from L to T and then to Y. However, the initial mass of the brown dwarf plays a key role in the initial temperature and the cooling rate. A more massive brown dwarf will have a hotter initial temperature than a less massive brown dwarf.

The L brown dwarfs are the hottest and youngest of the three spectral types, with temperature ranging from 1400-2600K. All but one of the first 26 dwarfs to be classified are L dwarfs(Kirkpatrick et al. 1999). The second spectra of Fig. 1.1 provides a sample of an L dwarf spectra in comparison to an M star, a T dwarf, and Jupiter. The L dwarf spectrum lacks the TiO bands found in the M star spectrum. Instead, a strong K I line is located at approximately 1.8 μm.

The T brown dwarfs are the next coolest objects, with temperatures between 600-1400K. Prominent methane bands distinguish T dwarfs from L dwarfs (Kirkpatrick et al. 1999). The methane bands occur throughout the spectrum of the brown dwarf. Refer back to Fig. 1.1 for a visual comparison with the spectrum of the L dwarf. In the warmer L dwarfs, CO dominates the atmosphere. As the star cools, methane forms in the reaction

$$CO + 3H_2 <=> CH_4 + H_20. \tag{1.1}$$

Warmer temperatures move the reaction to the right-hand side, while temperature below 1400 K move the reaction to the left-hand side. The cooler the dwarf becomes, the faster the reaction is able to occur, eventually eliminating the CO and populating the spectrum with methane lines.

The Y dwarfs are the coolest and oldest of all three classifications, with temperatures from 350-600 K. The spectra for these objects would lie between the spectra of the T dwarfs and Jupiter in Fig. 1.1. These objects become cool enough, that N_2 can react with H to begin forming ammonia in the reaction

$$N_2 + 3H_2 <=> 2NH_3. \tag{1.2}$$

As the dwarf cools, this reaction creates more ammonia. Due to ammonia and methane absorption, Y dwarfs are very dim, even in the infrared. Only six Y dwarfs have been observed and classified as of the publication of this thesis (Cushing et al. 2011).

1.3 The Cooling Model

1.3.1 Current Theory of Cooling

In order to better characterize brown dwarfs, a theoretical cooling model has been created. The model, shown in Fig. 1.2, allows the mass of a brown dwarf to be estimated based on known age and luminosity. To better understand formation and evolution of brown dwarfs, we need to know

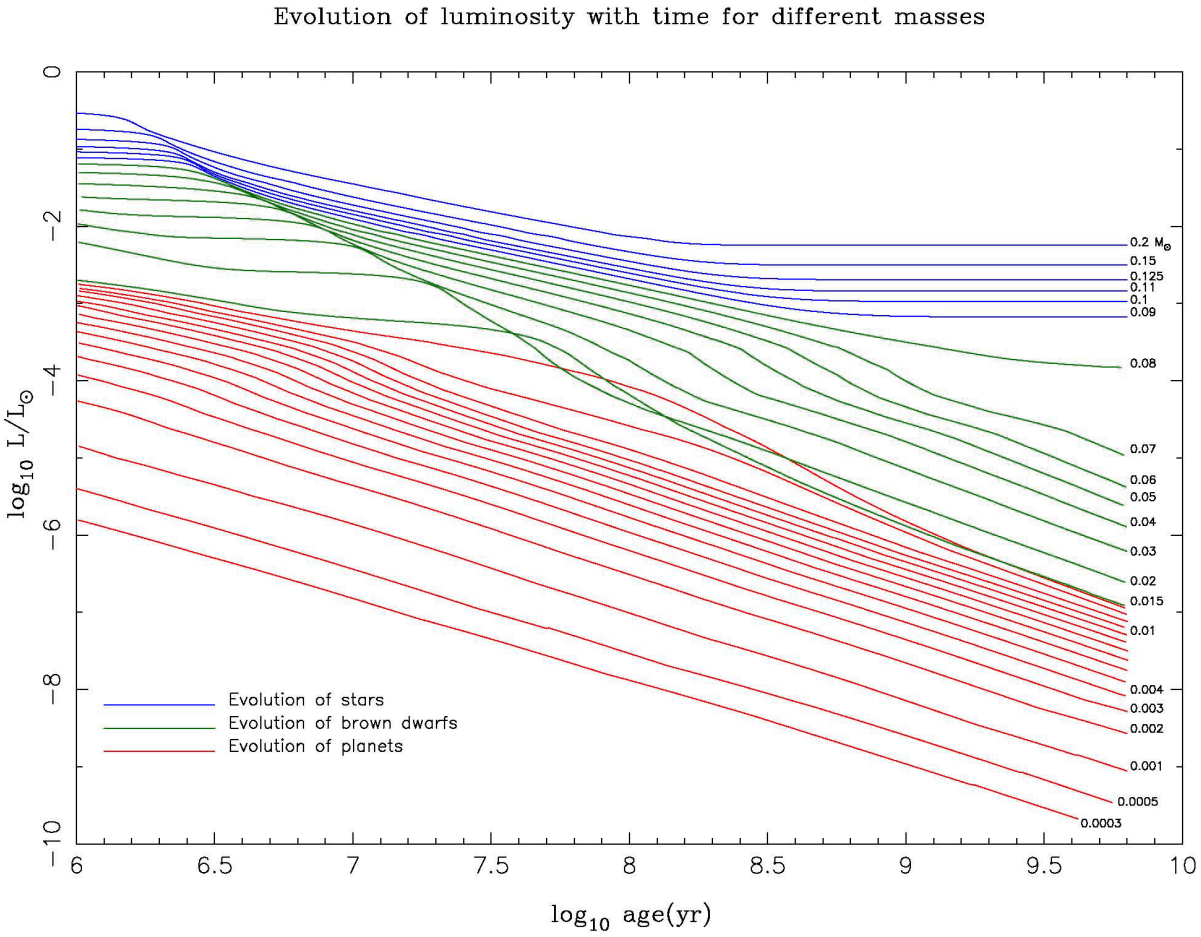

Figure 1.2 The changes in luminosity of stars (0.09 $M_{\odot}$ and greater), brown dwarfs (0.015-0.08 $M_{\odot}$), and planets (less than 0.015 $M_{\odot}$). Stars, which have a mass greater than 0.09 $M_{\odot}$, dim briefly before reaching a constant luminosity. Brown dwarfs and planets both continue to diminish in luminosity as they age (Burrows 1999).

their mass. For example, by comparing the isochrone of a given mass with the luminosity of a given object, we can determine if the object is an old, large dwarf which is still bright because of its size, or if it is small and young, therefore still very luminous (Dupuy 2011).

Unfortunately, as we compare calculated masses of six brown dwarfs to the model, they frequently disagree. A new model needs to be created (Dupuy et al. 2014). The present number of

brown dwarfs for which we have a known mass is too small and does not provide the data needed to create a new cooling model.

1.3.2 Mass and Binary Systems

In order to find a more accurate cooling model for brown dwarfs, there needs to be a greater database of objects with known characteristics such as age, mass, and luminosity. Unfortunately, brown dwarfs are difficult to observe due to their low luminosity.

The age and luminosity of a brown dwarfs can be determined when a brown dwarfs is located in the proximity of a main-sequence star. Stellar objects in close proximity generally form around the same time. The main-sequence star follows a well-tested evolutionary pattern, allowing us to easily determine the age and distance of the star. Using the distance to a star or brown dwarf, the absolute magnitude—or actual brightness—can be calculated.

Determining mass, however, requires two objects to be close enough to each other to have a gravitational interaction, orbiting each other as a binary system. In addition, the mass can be more accurately measured if the two objects have similar mass. A brown dwarf which is at a substantial distance from a large star will have little gravitational effect on the star. A brown dwarf in a close binary system with another brown dwarf provides the best opportunity to determine the mass of both objects.

1.3.3 Point-Spread Functions

The small size of brown dwarfs allows binary brown dwarf systems to have small separations. Prior to powerful space-based telescopes, many binary systems were observed as single objects due to this small separation. The Hubble Space Telescope (HST) revealed many of these objects to be binary systems. However, even HST is not capable of resolving all binary systems; some objects are just too close to each other.

I have assisted in testing a program which determines the probability that a known brown dwarf is actually a binary brown dwarf system using point-spread function (PSF) modeling of HST data sets. A PSF is the pattern recorded by the camera of a telescope which is created by a point source, a single object such as a star or brown dwarf. Essentially, it is a two-dimensional distribution of the light from the object.

A PSF is dependent on three things, the object, the filter, and the camera. First, the brightness, chemical composition, and temperature of an object all influence the light which is emitted. Second, a filter limits the light which reaches the camera. Finally, each camera reacts differently to the light it receives. These three things determine the PSF which can be used to analyze an image. The unique nature of the PSF allows us to create models using both individual PSFs and pairs of PSFs and compare the models to actual images available in the HST archives. Each model creates a slightly different image. The closest match can be considered a more accurate representation of the object.

1.4 Brown Dwarf 2M 0559

Many brown dwarf astronomers have speculated that 2M 0559 is actually a binary system, yet it is visually unresolved according to the Rayleigh Criterion, even in instruments such as HST. This object has a spectral type of T4.5, a classification which generally has an absolute magnitude of 14. However, 2M 0559 has an absolute magnitude of 13, nearly two and a half times brighter due to the logarithmic nature of the magnitude scale. This implies that there may be a second object contributing additional light to the images.

1.5 Previous Work at Brigham Young University

Prior to our study of brown dwarfs, Denise Stephens used PSF-fitting to find binary Trans-Neptunian objects (TNOs). In order to locate potential binary systems among the TNOs, Stephens designed a point-spread function (PSF) fitting program. This program analyzed the light curves in the observations of TNOs and returned probably binary results for the objects.

Stephens recognized the potential of applying this program to brown dwarfs in order to expand the limited database of binary brown dwarf systems. Jacob Albretson, a BYU graduate student, applied this program to observations of ten brown dwarfs in the HST database. Albretson's research determined that the PSF-fitting program could be used on brown dwarf data. Of the ten objects he analyzed, two returned results indicating a high probability of binarity. The other eight exhibited very low probability of being binary systems, implying that the objects studied are, in fact, single objects. All data from Albretson's research were collected using the Near Infrared Camera and Multi-Object Spectrometer (NICMOS) 2, analyzing only four images for each object. Albretson did not conduct any follow-up analysis on the two potential binary systems. One of these objects is 2M 0559.

After Albretson's work on binary frequency of brown dwarfs, how often brown dwarfs appear to be binary, Taren Esplin, a BYU student, began a deeper analysis of 2M 0559, focusing on the spectrum of 2M 0559. This object already had a known spectral type of T4.5. Using the spectrum of 2M 0559, Esplin analyzed model spectra over a range of temperature, gravity, and cloud opacity. By combining the spectra of two different models, Esplin found many potential spectral combinations which would produce a combined spectrum similar to that of a T4.5 brown dwarf. However, Esplin's work returned several potential binary solutions. At the time, there were no constraints on the flux of either the primary or the secondary object, should the system be binary, so all results found by Esplin's work were equally probable (Esplin 2010).

1.6 Overview

1.6.1 Procedures

In Chapter 2, I will present the procedure for using the PSF-fitting program. I will explain how data is prepared for analysis by the program. I will then describe how the program is used to find optimal solutions for both a binary and a singular fit, as well as the comparison of both results to find the best fit. Finally, I will present a summary of work completed by Douglass Gardner to determine the limits and validity of this procedure.

1.6.2 Results and Conclusions

According to the procedure described in the Chapter 2, 2M 0559 is a strong binary candidate. In Chapter 3, I will present a comparison of the binary fit with the singular fit found by our program. In addition to this, I will present approximate magnitudes found for both the primary and secondary objects. I also describe future work my adviser and I intend to do with the data in order to further strengthen the argument that 2M 0559 is binary and to begin to determine orbital periods and masses of the system.

Chapter 2

Procedures

2.1 Preparing Data for Analysis

2.1.1 Data Collection

Due to the controversial nature of 2M 0559 described in Section 1.3, a great deal of data has already been collected for this object with HST. Additional data has been collected because HST uses 2M 0559 as a standard test due to the object being bright and very red.

We collected all available data from the HST archives for 2M 0559. The dates for these observations range primarily from 2001 to 2004, with additional data sets in 2007 and 2013. Data was collected with the following cameras: Near Infrared Cameras and Multi-Object Spectrum 1 and 2 (NICMOS1 and NICMOS2), the Wide Field and Planetary Camera 2: Planetary Camera 1 and Wide Field Camera 3 (WF/PC2.pc1 and WF/PC2.wf3), and the Wide Field Camera 3(WFC3). This collection extends through both the infrared range with NICMOS1, NICMOS2 and WFC3 and the visible range with WFPC2. This paper focuses on the data from 2003-2004 in NICMOS1 and NICMOS2. Table 2.1 contains a list of the available data and the associated filters and cameras.

Filter (peak-wavelength)	Camera	Date	Images Analyzed vs. Available Images
f814w	WF/PC2.pc1	6 Sep 2000	0/2
f1042m			0/2
f110w	NICMOS2	23 Jan 2003	2/2
f180m			2/2
f207m			2/2
f222m			2/2
f090m	NICMOS1	22 Aug 2004	3/26
f110m			3/12
f145m			2/12
f165m			2/12
f207m	NICMOS2	22 Aug 2004	3/14
f222m			4/14
f108n	NICMOS1	7 Sep 2004	4/4
f113n			4/4
f785lp	WF/PC2.pc1	22 Oct 2004	0/2
f791w			0/2
f814w			0/2
f850lp			0/2
f1042m			0/3
f814w	WF/PC2.wf3	16 Dec 2007	0/2
f850w			0/2
f1042m			0/2

Table 2.1 Available data sets for 2M 0559, sorted by observation date. WFC3 data is not yet requested and therefore not yet listed.

	140	141	142	143	144	145	146	147	148	149	150
82	0.022	-0.006	0.02	0.051	0.087	0.11	0.061	0.035	-0.02	-0.03	-0.02
81	0.046	-0.01	0.071	0.293	0.322	0.367	0.373	0.259	0.14	0.064	-0.02
80	0.087	0.004	0.311	0.678	0.551	0.408	0.505	0.779	0.679	0.062	0.019
79	0.087	0.1	0.447	0.459	0.454	1.225	0.763	0.533	0.695	0.104	0.084
78	0.028	0.12	0.451	0.314	2.225	5.643	2.825	0.366	0.454	0.166	0.025
77	0.031	0.074	0.408	0.26	2.465	7.185	4.032	0.402	0.554	0.22	0.073
76	-0.02	0.055	0.494	0.42	1.052	2.651	1.407	0.346	0.733	0.217	0.027
75	0.03	0.034	0.448	0.789	0.593	0.471	0.354	0.679	0.575	0.111	0.02
74	0.059	0.144	0.217	0.457	0.393	0.357	0.298	0.393	0.251	-0.03	-0.04
73	0.037	0.027	0.082	0.046	0.125	0.16	0.052	-0.02	0.03	0.008	0.009
72	-0.006	0.046	0.054	0.06	0.021	0.113	0.09	0.049	-0.04	-0.04	-0.03

Figure 2.1 The number grid presents flux count for individual pixels in an image. The top-most row is the x position of each pixel and they right-most column is the y position of each pixel. The light in this image is primarily in (145,77), so a 5x5 region of interest around this pixel is selected for in-depth analysis. The remaining pixels contain only background noise, normalized to an average value of 0, allowing some pixels to contain negative numbers.

2.1.2 Preparation

Tiny Tim is a program which can create PSFs for nearly all camera/filter combinations available for HST (Krist & Hook 2003). Using this program and the known spectrum of 2M 0559, I created unique model PSFs for 2M 0559 for each camera and filter combination for which I had data.

After creating the model PSFs, I selected a region of interest to constrain the program to exclude pixels which contain only background noise. Because 2M 0559 is both small and dim, we can focus on a small range of pixels instead of attempting to analyze a large image. Figure 2.1 depicts a typical region of interest which contains a 5 pixel by 5 pixel square, centered on the pixel which contains the bulk of the flux from the object.

Additional preparation for this project includes modifying the original PSF-fitting program, which was designed to work with NICMOS2, to also analyze NICMOS1 data.

2.2 Procedure for a Binary PSF Fit

Here is a brief summary of the procedure followed by the PSF-fitting program to find a binary PSF fit. A more detailed description of this procedure can be found in the Stephens and Noll paper from 2006 (Stephens & Noll 2006).

2.2.1 Weighting

In order to assist the program in properly positioning the secondary PSF, the importance of each pixel is weighted according to the square-root of the total flux in the pixel. This weighting is necessary due to the small size and low flux of the brown dwarfs. The images taken by HST are considered to be under-sampled, meaning nearly all the flux is found in one or two pixels, with low flux counts in the neighboring pixels and only background noise in the remainder of the image (Howell et al. 1996). This places essentially all the flux in one to four pixels, depending on the exact location of the star within the pixel. This can be seen in Fig. 2.1, where pixel (145,77) and (145,78) contain much more flux than the remaining pixels in the region of interest.

By weighting the pixels according to the square-root of their flux, the intermediary pixels, which are most likely to contain the secondary object, are given greater importance in the PSF-fitting, better enabling the program to locate the secondary. Without the weighting, pixel (145,77) would have a natural weighting of 7.185 compared to a natural weight of 2.465 for pixel (144,77). The implemented weighting minimizes (145,77) to a weight of 2.68 while only lowering (144,77) to 1.57. It should be noted that the program uses this weighting to position the model PSFs, not to analyze the accuracy of the binary solutions found.

2.2.2 Positioning the Binary Fit

For each pixel within the region of interest, the program considers a 0.1 pixel grid containing 100 model PSFs. The 100 sub-pixel grid on the PSF enables the program to match a more accurate binary PSF model of the object to the data because each model reveals minor alterations in surrounding pixels (Howell et al. 1996).

The program examines all pairs of possible positions for the primary and secondary object. For each pair of positions, overall flux is maintained at the value of the image while scaling the flux of each PSF. The program determines the χ^2 value by subtracting the two model PSFs for each combination of flux values from the image data (Stephens & Noll 2006). The fit with the smallest χ^2 for each set of positions is saved as the program iterates through all possible pairs.

After iterating through all positions, the PSF-fitting program returns the χ^2, positions, fluxes, separation, and position angle of the 12 best binary models for the image. The position pair and flux value with the lowest overall χ^2 is considered the most optimal binary model for the object.

This procedure is considered a "brute-force" procedure because the program tests every possible binary model within the constraints of the image. The brute-force procedure is possible with brown dwarfs due to the under-sampled nature of the data, or rather, the image having minimal flux counts in merely a handful of pixels. By taking this approach instead of a more traditional fitting-program, we reduce the occurrence of false positives. The program cannot get caught in a local minimum because every single location is tested anyways.

2.3 Procedure for a Singular PSF Fit

I used a similar PSF-fitting program to determine the most optimal singular fit of the object. This program positions a single PSF model using the same grid described for the binary fit. The program does not use scaling for the flux in this procedure because the total flux of the image needs to be

accounted for in the model.

For the singular fit, the program only returns the χ^2 and the flux of the object.

2.4 Use of Data from Both Procedures

2.4.1 Comparison

I compared the χ^2 values from the optimal fit returned by both procedures in order to determine which of the fits best describes the system. If the χ^2 of the binary fit is smaller than the χ^2 of the singular fit by a factor of three or more, the object is declared to be a binary system. Otherwise, the test is considered to be inconclusive.

When the program returns inconclusive results, the data returned will be analyzed by a Monte-Carlo simulation, described in Section 2.5. This simulation places upper limits on the flux and separation of potential companions.

2.4.2 Preliminary Analysis

After declaring an object to be a binary system, I analyzed the additional information returned by the PSF-fitting program to determine characteristics of both the primary and secondary object. Using this flux, I calculated magnitudes of both objects. Katrina Wright is conducting fitting of model spectra to 2M 0559 using this data as constraints (Wright 2015).

2.5 Reliability of the Procedures

Doug Gardner has developed a Monte Carlo program to test the PSF-fitting program that has been described here. His program creates millions of fake binary systems, generates and applies both background and Poisson noise to create realistic images, and then runs each of the fake binary

systems through the binary and singular fit programs. The frequency with which a binary system is correctly returned determines the ability of the PSF-fitting program to properly find the binary fit for various magnitudes, separations, cameras, and filters. Further details of his work are presented in Gardner's thesis (Gardner 2015).

Chapter 3

Results and Conclusions

3.1 2M 0559 is a Strong Binary Candidate

The χ^2 for the binary fit for 2m 0559 is better than the χ^2 for the singular fit, ranging from a factor of 3-17 depending on the camera and filter being analyzed, shown in Table 3.1. 2M 0559 is strong binary candidate.

Figures 3.1- 3.2 visually depict the residuals for 2M 0559 for different cameras and filters. Both figures contain 4 images: the original image, an image with the primary PSF subtracted out in order to see the secondary object, the residual left after subtracting both PSFs from the optimal binary fit, and the residual left after subtracting the PSF from the optimal singular fit. The plate scaling in these two figures is set to emphasize differences in flux between pixels.

A comparison of Fig. 3.1c to Fig. 3.1d, or a comparison of Fig. 3.2c to Fig. 3.2d, visually demonstrates that the binary fit is more accurate than the singular fit. Though the binary fit is not perfect, revealing a few pixels which retain too much residual light, the residual of the singular fit reveals substantial amount of light from the secondary object.

Comparing Fig. 3.1c to Fig. 3.2c reveals the difference in the accuracy of the PSF-fitting pro-

Filter	Camera	Binary χ^2	Singular χ^2	Ratio
f090m	NICMOS1	0.8161	3.9300	4.8156
f108n	NICMOS1	0.0330	0.5803	17.5599
f110m	NICMOS1	114.1490	403.7362	3.5369
f110w	NICMOS2	198.1817	1570.3603	7.9238
f113n	NICMOS1	0.0087	0.1028	11.8626
f145m	NICMOS1	16.7636	95.2652	5.6828
f207m	NICMOS2	8.4108	49.0418	5.8308
f222m	NICMOS2	1.2617	7.8750	6.2418

Table 3.1 A comparison of the χ^2 value of the optimal binary and singular PSF fit for a sample of the images analyzed, organized based on peak wavelength of the filter. The narrow filters, f108n and f113n, focus on a more limited range of wavelengths, this enables the filter not only to find a more accurate fit for both models but to demonstrate the binary characteristics within the image.

gram for different cameras and different filters. The difference between the two cameras is caused by different plate scales. NICMOS1 has a plate scale of 0.043"/pixel, but NICMOS2 has a much larger plate scale of 0.075"/pixel. Data taken with NICMOS2 is more likely to have both objects fall within the same pixel or barely across the border of two pixels. The close proximity of the two objects in the image inhibits the program from finding an optimal binary fit for the system. In NICMOS1 images, the two objects are farther apart in the image, allowing the program to more easily find an optimal binary fit.

In addition, the PSF-fitting program returns a more accurate result for shorter wavelengths. 2M 0559 becomes brighter in the far infrared range. As a result, over the range of wavelengths tested, 0.9 μm through 2.2 μm, the overall flux of 2M 0559 increases for longer wavelengths. The increase in flux causes the light from both objects to bleed into each other, washing out features which would enable the program to accurately determine the best fit. The NICMOS1 results presented in

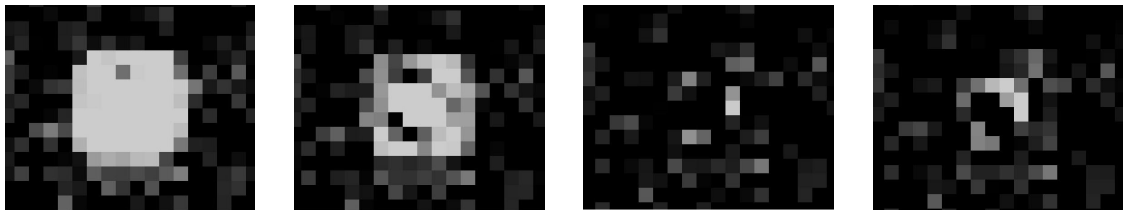

(a) Original HST Image

(b) Residual image after subtraction of the primary object from the binary fit

(c) Residual image after subtraction of the binary fit

(d) Residual image after subtraction of the singular fit

Figure 3.1 2M 0559 imaged with NICMOS1, filter f090m. The subtraction of the primary object in Figure (b) reveals the secondary light source. Figures (c) and (d) provide a visual comparison of the residuals of both the binary and the singular fit.

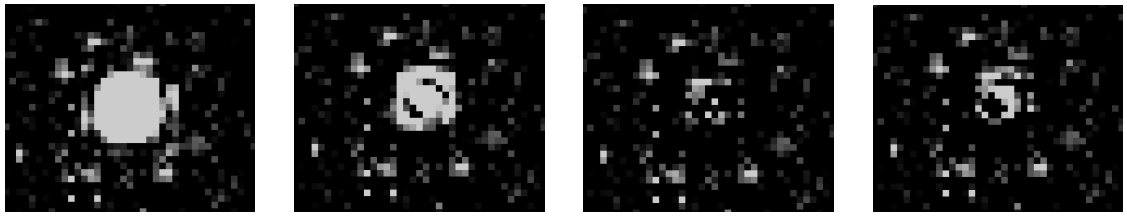

(a) Original HST Image

(b) Residual image after subtraction of the primary object from the binary fit

(c) Residual image after subtraction of the binary fit

(d) Residual image after subtraction of the singular fit

Figure 3.2 2M 0559 imaged with NICMOS2, filter f207m. These images follow the same description as in Fig 3.1.

Fig. 3.1 were gathered with a f090m filter, meaning the light collected was of wavelengths at and around 0.9 μm. NICMOS2 results presented in Fig. 3.2 are more than twice the wavelength using the f207m filter, so the primary wavelength observed was 2.07 μm. Both increased flux and plate scale contribute to the greater residual scene in the NICMOS2 results.

The visual comparison of residuals also demonstrates the accuracy of results returned by the program for apparently single brown dwarfs, 2MASS J03370359-1758079 (2M 0337). Figures 3.3-3.4 compare the results of 2M 0559 with 2M 0337. These image sets follow the same pattern as the two figures discussed previously. However, both of the original images for these fig-

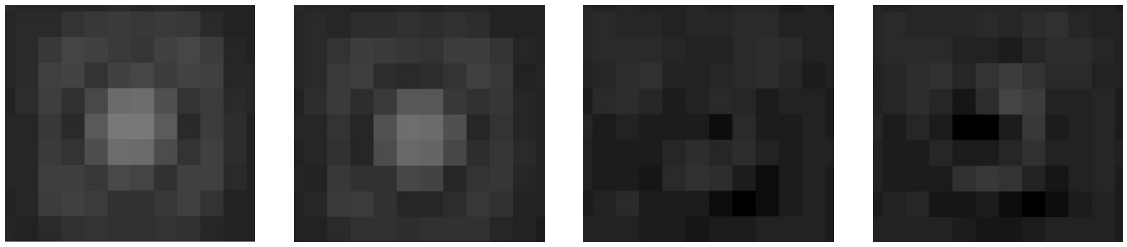

(a) Original HST Image of 2M 0559

(b) Residual image after subtraction of the primary object from the binary fit

(c) Residual image after subtraction of the binary fit

(d) Residual image after subtraction of the singular fit

Figure 3.3 By using a logarithmic pixel scale, this figure visually demonstrates that for both the binary and singular fit, the residual is close to the background level of the image. In this set, the binary fit is better than the singular fit.

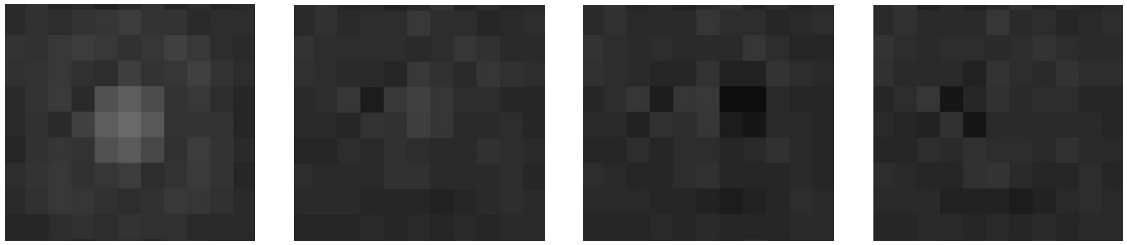

(a) Original HST Image of Single object

(b) Residual image after subtraction of the primary object from the binary fit

(c) Residual image after subtraction of the binary fit

(d) Residual image after subtraction of the singular fit

Figure 3.4 A logarithmic scale to accurate depict the difference between background levels and residuals. This set demonstrates that the single fit is better than the binary fit.

ures were taken with NICMOS2 in the f110w filter. The pixel scale in these images are logarithmic to show that for both objects and for both singular and binary fits, the residual pixels are relatively close to the background level of the image. These images show that the model for the less-likely fit frequently contains too much flux and over-subtracts from the original image.

An analysis of Fig. 3.3c and Fig.3.3d again reveals that, for 2M 0559, the residual from the binary fit is much better than the residual from the singular fit. Fig. 3.4c and Fig.3.4d, display the opposite pattern, which is expected because these images are of 2M 0337, an apparently single

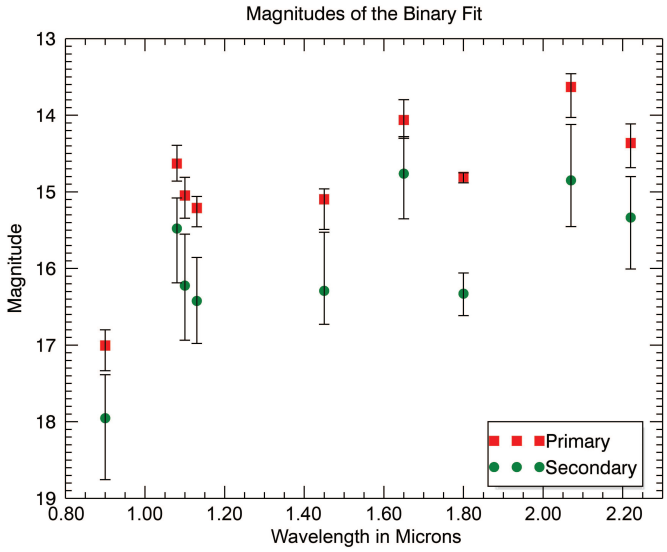

Figure 3.5 Magnitudes of the primary and secondary object as found by the PSF-fitting program. The wavelength of each data point corresponds to the central wavelength of the filter. The magnitude is the average magnitude found from all the images of the object in a given filter. The error bars represent the range of magnitudes returned for the 5 best binary fits for each image in each filter

object. In this case, the single residual is significantly better than the binary residual, which over-subtracts a large portion of the object. Due to noise, neither model is a perfect fit for either image.

Using the flux returned returned by the PSF-fitting program, I found the magnitudes of both the primary and secondary objects for the binary fit for each filter in the NICMOS1 and NICMOS2 cameras. These magnitudes are shown in Fig. 3.5. In most filters, the secondary object is dimmer than the primary by about one magnitude. However, from 1.6 μm to 1.8 μm, the two objects differ by nearly two magnitude.

3.2 Magnitude and Spectra of 2M 0559

The changes in magnitude can be compared to the spectrum in Fig. 3.6 to approximate the spectral type of each object in the binary system. The spectrum of 2M 0559, a T4.5 dwarf, is shown second

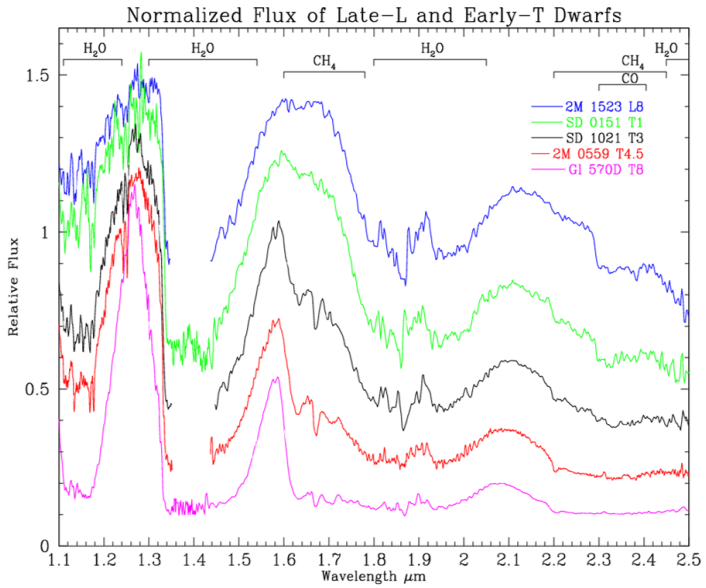

Figure 3.6 Spectra of 5 brown dwarfs. The overall spectrum 2M 0559 is the second spectrum from the bottom of the graph. Methane absorption, which is more prominent at cooler temperatures, causes the flux to dimension from 1.65-1.8 μm. Infrared spectra were taken from several sources: 2M 0559, SD 0151, 2M 1523 (Geballe et al. 2002); SD 1021 (Leggett et al. 2000); GI 570D (Geballe et al. 2001)

from the bottom. The uppermost spectrum, the spectrum of an L8 dwarf, has a thick methane band from 1.5-1.8 μm. This band narrows to a small peak in the cooler dwarfs. As a brown dwarf cools, methane becomes a more prominent molecule in the dwarf's atmosphere. As more methane accumulates in cooler dwarfs, the methane eventually absorbs all the flux from approximately 1.65 to 1.8 μm.

The decrease in flux above 1.65 μm places constraints on the possible spectral types of the primary and secondary dwarf of 2M 0559. The primary object dims slightly at 1.8 μm, so it probably has a spectral type near T3. The secondary object, however, dims substantially at 1.8 μm. This dwarf probably has a spectral type of T5. A T5 spectrum is shown in Fig. 1.1.

3.3 Conclusions

According to the constraints of the PSF-fitting program, 2M 0559 is a binary object. For all filter and camera types, the binary fit is more accurate than the singular fit by a factor of three or more.

The spectral type of the primary is approximately T3, based on the small decrease in magnitude between 1.6 μm and 1.8 μm. The secondary object of the binary system has an approximate spectral type of T5, based on a substantial decrease in magnitude between 1.6 μm and 1.8 μm, especially in comparison to the primary object.

3.4 Direction for Further Work

Presently, I have only analyzed the residual values and the flux returned by the PSF-fitting program. Additional parameters returned by this program include separation and position angle. We intend on analyzing these two parameters in order to determine the orbital period of 2M 0559. Determining the orbital period will allow us to calculate relative masses of the two objects.

As mentioned in Section 2.1, this work focused on data gathered by HST using NICMOS1 and NICMOS2. We intend to further modify the program to analyze WF/PC2 and WFC3 data in order to expand the range of plate-scales, wavelengths, and dates of analyzed data. A greater range of wavelengths will increase the range for which we have magnitudes, providing additional constraints to determine spectral types of the primary and secondary object. An increase in the range of dates provides more opportunities to measure changes in position angle, improving the chance of calculating the orbital period of the binary system, ultimately leading to determining the masses for the binary system.

The program also needs to be modified to return actual error for the values returned. Presently, error bars are calculated using the average values given for the five best binary fits for each camera and filter set. The potential error on the actual value returned by the optimal binary fit has not yet

been calculated.

Bibliography

Burrows, A. 1999

Cushing, M. C., et al. 2011, The Astrophysical Journal, 743, 50

Dupuy, T. J. 2011, arXiv, 1103, 5747

Dupuy, T. J., Liu, M. C., & Ireland, M. J. 2014, The Astrophysical Journal, 790, 133

Esplin, T. L. 2010, Statistical Spectral Fitting of the Brown Dwarf Binary System 2M0559, Bachelors Thesis (Brigham Young University)

Gardner, D. B. 2015, In Preparation, Bachelors Thesis (Brigham Young University)

Geballe, T. R., et al. 2001, The Astrophyscial Journal, 556, 373

—. 2002, The Astrophyscial Journal, 564, 466

Howell, S. B., Koehn, B., Bowell, E., & Hoffman, M. 1996, The Astronomical Journal, 112, 1302

Kirkpatrick, J. D., et al. 1999, ApJ, 519, 802

Krist, J. E., & Hook, R. 2003

Kumar, S. 1963, ApJ, 137, 1121

Leggett, S. K., et al. 2000, The Astrophyscial Journal, 536, L35

Marley, & Leggett. 2009, Procedures of Astrophyscis in the Next Decade, 101

Stephens, D. C., & Noll, K. S. 2006, The Astrophyscial Journal, 131, 1142

Wright, K. 2015, In Preparation, Bachelors Thesis (Brigham Young University)

Index

2M 0559, 1, 8

binary system, 7
brown dwarf, 1

cooling model, 5–7
core-fusion, 2, 3

Hubble Space Telescope, HST, 7, 8, 11, 14, 24

isochrone, 6

light curve, 9

NICMOS1, 11, 13, 19, 22, 24
NICMOS2, 11, 13, 19–22

point-spread function, PSF, 8, 13–15

spectral classification, 3–5, 8

WF/PC2, 11, 24
WFC3, 11, 24